Magneto-Optical-Trap-Based, High Brightness Ion Source for Use as a Nanoscale Probe

James L. Hanssen[1,*], Shannon B. Hill, Jon Orloff[2], and Jabez J. McClelland

Center for Nanoscale Science and Technology, National Institute of Standards and Technology,

Gaithersburg, MD 20899, USA

james.hanssen@nist.gov

[1] also Maryland NanoCenter, University of Maryland, College Park, MD 20742, USA and Center for Nanoscale Science and Technology, National Institute of Standards and Technology, Gaithersburg, MD 20899, USA.

[2]FEI Company, Hillsboro, OR, 97124, USA.

ABSTRACT: We report on the demonstration of a low emittance, high brightness ion source based on magneto-optically trapped neutral atoms. Our source has ion optical properties comparable to or better than those of the commonly used liquid metal ion source. In addition, it has several advantages that offer new possibilities, including high resolution ion microscopy with ion species tailored for specific applications, contamination-free ion milling, and nanoscale implantation of a variety of elements, either in large quantities, or one at a time, deterministically. Using laser-cooled Cr atoms, we create an ion beam with a normalized *rms* (root mean square) emittance of 6.0×10^{-7} mm mrad $\sqrt{\text{MeV}}$ and approximately 0.25 pA of usable current, which with optimal apertures could yield a brightness as high as 2.25 A cm^{-2} sr^{-1} eV^{-1}. These values of emittance and brightness show that, with suitable ion optics,

an ion beam with a useful amount of current can be produced and focused to spot sizes of less than 1 nm.

MANUSCRIPT: As a tool, the focused ion beam (FIB) has led to great advances in the field of nanotechnology [1, 2]. A FIB relies on a high brightness source to create a tightly focused ion beam that can be used for a variety of tasks on the nanometer scale [3]. The clearest demonstrations of this have been in the realm of nanoscale fabrication and characterization. A number of extremely useful techniques are in widespread practice today, such as ion milling, where material is removed, chemical vapor deposition, where material is deposited, and microscopy, where secondary electrons are generated and collected as the beam is scanned. These techniques enable creation of nanometer-scale devices and production of high resolution images.

Current technology, however, is limited by a number of factors. The vast majority of applications of FIBs today use a field emission liquid metal ion source (LMIS), which is practically limited to a single heavy metal ionic species, Ga^+. Due to its large mass, Ga^+ has a high sputtering rate, which is good for ion milling but not for microscopy. Counterintuitively, it is possible to use ion milling to create a structure with a Ga^+ LMIS FIB that is smaller than can be reliably imaged with the same FIB because of this sputtering problem [4]. This is unfortunate because highly focused ions are potentially superior to electrons in scanning microscopy applications since secondary electrons are produced right at the point of impact instead of deep within the sample [4]. Another disadvantage of Ga^+ that is a significant problem for both milling and imaging is the implantation of Ga^+, which can introduce an unacceptable level of contamination in the sample.

Recently, high brightness gas field ionization sources have been introduced that address some of the issues associated with Ga^+ [5, 6]. However, these sources have been limited to a few light species such as H_2^+, He^+ and Ne^+, and high brightness has been elusive except in the case of He^+ [7]. While these

sources hold promise for expanding the usefulness of focused ion beams, new problems are also being discovered, such as material swelling on the nanometer scale due to implantation of inert gas ions [8].

For these reasons it is desirable to have a high brightness ion source that can produce a wide variety of ionic species, from low-sputter-yield light ions, to non-contaminating heavy ions. Such an ion source would greatly expand the usefulness of ion microscopy, eliminate sputtering problems and possibly introduce new contrast mechanisms based on specific ion-target interactions. It would also allow unprecedented control over contamination through judicious choice of ionic species.

In this letter, we report on the demonstration of a novel ion source based on laser-cooled atoms that has both low emittance and high brightness. We have built an experimental realization of a magneto-optical trap ion source (MOTIS) [9, 10,11] in a system designed specifically to determine small emittances. Our determinations of the emittance and brightness of this new source show values that are comparable to those found in other high brightness sources such as the LMIS. These results indicate that the MOTIS is an ion source that has great potential for enabling new forms of microscopy and nanofabrication.

The fact that the MOTIS makes use of laser-cooled and trapped neutral atoms allows for a range of new capabilities not available with other ion sources. For example, many different atomic species, such as noble gases, alkali metals, and some transition metals, can be used in the source, all with similar emittance and brightness. This is a significant advantage over other sources because it enables the tailoring of ion-sample interactions, depending on the specific application. Light ions can be chosen to optimize microscopy; heavy, inert ions can be selected to optimize ion milling; or specific reactive ions can be used to enable new contrast mechanisms or nanoscale localized chemical reactions. Further advantages of the source include a low current density at the source, which significantly reduces space charge interactions, an inherently narrow energy spread, an ability to be used as either an ion or electron source, and a capability of being used as a deterministic single ion source which could allow single ion doping with nanometer resolution [12].

In any ion source, emittance and brightness are the two fundamental quantities that characterize the ability to create small focal spots with enough current to be useful. Emittance is a measure of the phase space volume occupied by the beam, and is defined in its normalized form as

$$\varepsilon_x = \iint \frac{dx \, dx'}{\pi} \sqrt{U},$$

(1)

where the integration is over position, x, and angle, x', for a specific fraction of the beam, and U is the energy of the beam [13]. The square root of the energy is used to normalize the emittance, making it an invariant along the focusing column. An alternate definition of the emittance based explicitly on the shape of the particle distribution in phase space is the *rms* emittance. It is defined as

$$\varepsilon_{rms,x} = \sqrt{\langle x^2 \rangle \langle x'^2 \rangle - \langle xx' \rangle^2} \sqrt{U}$$

(2)

where $\langle x^2 \rangle$, $\langle x'^2 \rangle$, and $\langle xx' \rangle$ are the different moments of the particle distribution in phase space [13]. This definition is useful from an experimental and numerical standpoint as these moments are readily measured or calculated. It can be shown that the normalized emittance is roughly equal to four times the *rms* emittance [13]. At the focus of an ion optical system, the emittance is simply the product of the beam width and the angular spread. Since the emittance is conserved throughout an ion beam, a determination of the source emittance is all that is needed to know the focal properties of the beam, as long as space charge and aberrations can be neglected. A low emittance means a highly focused beam can be achieved.

Because the emittance depends on source area, it is possible to reduce the emittance to an arbitrarily low value by aperturing the beam. However, this is done at the expense of beam current, and hence, is not always a practical option. The brightness of the beam gives a measure of how much current can be concentrated in a small spot, and is defined as

$$B = \frac{\partial^2 I}{\partial A \partial \Omega} = \frac{I}{8\pi^2 \varepsilon_{rms,x} \varepsilon_{rms,y}},$$

(3)

where I is the beam current, A is area, and Ω is solid angle [13]. Like the emittance, the brightness is an invariant along the beam path, and higher brightness is associated with a higher performance beam.

4

The LMIS achieves its low emittance and high brightness by emitting a large amount of current from a very small effective source. Typical sources have a virtual size of about 50 nm and emit up to 10 μA of current into a half angle of approximately 20 degrees [4,14]. Usually the beam is apertured to a current of ≈ 10 pA and a half angle of ≈ 0.5 mrad. These parameters correspond to a theoretically predicted emittance of 1.1×10^{-6} π mm mrad $\sqrt{\text{MeV}}$ and a brightness of 10 A cm^{-2} sr^{-1} eV^{-1} to 100 A cm^{-2} sr^{-1} eV^{-1} [15, 16, 17].

The MOTIS achieves low emittance from a different perspective. Instead of using a small source size to reduce the emittance, the MOTIS uses small angular spread to achieve the same result. This small angular spread is attained by starting with a magneto-optical trap (MOT), which uses laser cooling to create a small, dilute cloud of neutral atoms at an extremely low temperature [18]. On converting these cold neutral atoms into ions and extracting them, a low temperature beam is created that has a small transverse velocity spread, and hence, a small angular spread. For the low temperatures typical of laser-cooled atoms, angular spreads as low as 10 μrad are possible. This small angular spread leads to a small emittance, despite a source size much larger than found in an LMIS. It has been calculated that for temperatures and source sizes routinely achieved in the laboratory, emittances as low as 3.3×10^{-7} π mm mrad $\sqrt{\text{MeV}}$ should be possible using a MOT as an ion source [9].

Low emittance is not sufficient to qualify the MOTIS as a good ion source. It must produce a useful amount of current as well. To produce current, the neutral atoms within the MOT are converted to ions via photoionization. The cooling process that takes place within the MOT relies on continual absorption and spontaneous emission of near resonant light. A photoionization laser is used to ionize the atoms that are in the excited state because of the cooling process. The amount of current that can be extracted from the source depends on the rate that ions can be created. If a small region within the MOT is defined as the ionization region, then the current extracted from the MOT is proportional to the diffusion of atoms into the ionization region [19] and is ultimately limited by the load rate of atoms into the MOT [9]. The rate of diffusion depends on the density of atoms in the MOT. Based on this, it has been calculated that for typical MOTs it should be possible to extract up to 100 pA of current or more.

5

This current estimate, when combined with the estimated emittance, implies that the source could have a brightness as high as 10^3 A cm^{-2} sr^{-1} eV^{-1}.

We have built an apparatus to investigate the emittance and brightness of a MOTIS. A schematic representation of the experimental apparatus is given in Figure 1. The system consists of the following elements: 1) a MOT for trapping and cooling a cloud of neutral atoms, 2) an ionization laser for converting the trapped neutral atoms into ions, 3) electrodes to extract the ions once they are created and form them into a beam, and 4) diagnostic equipment to measure the beam current and the spatial profile of the beam. Each of these components will be discussed in detail in the following paragraphs.

The MOT in our experiment uses chromium atoms [20]. Chromium was chosen for this demonstration solely because the lasers and atomic source were already in place in our laboratory. Based on our understanding of the MOTIS, other species are expected to perform similarly or even better in many cases. The physics involved with creating a MOT as well as experimental details associated with typical traps can be found in Reference [21]. In steady state without extracting ions, we typically collect about 3300 atoms in a spherically symmetric cloud with a $1/e^2$ radius of approximately 150 μm, giving a peak density of $(5\pm1)\times10^8$ atoms cm^{-3}. The peak density of the MOT is determined by several parameters which we have optimized to reach maximum densities of $(1.5\pm0.3)\times10^9$ atoms/cm^3. The atoms within the trap have a temperature of (120 ± 50) μK, measured by free expansion of the atoms.

Production of Cr ions is achieved through photoionization [22] by using a single tunable ultra-violet (UV) laser with a wavelength sufficient to ionize only the excited-state neutral Cr atoms in the MOT. The threshold wavelength for ionization of atoms in the excited $4p\,^7P_4^o$ state of chromium is 321.78 nm. Photons with a longer wavelength would not have sufficient energy to ionize the atoms. Using a shorter wavelength would ionize the neutral atoms, but doing so would add energy into the resulting electron-ion system. For example, setting the ionization laser at a detuning $\Delta\lambda = 1.0$ nm below the threshold wavelength would result in an additional kinetic energy of 1.5 mK for the ions. The beam has a

6

maximum power of approximately 4 mW and has a $1/e^2$ waist of (10.0 ± 0.3) μm at the focus which is aligned to intersect the center of the MOT. This corresponds to a depth of focus of (1.96 ± 0.12) mm which is much greater than the $1/e^2$ diameter of the MOT. So the size of the ionization beam is essentially constant through the entire atom cloud.

It should be noted that there are other means of extracting ions from a cloud of cold neutral atoms. One route is to convert the atoms in the MOT into a plasma [23] and then extract ions. It has been observed that both ions and electrons created this way have a much higher temperature than the original cloud of laser-cooled neutral atoms, most likely due to plasma dynamics [24]. In that experiment, the ion beam had a measured transverse temperature of 60 K leading to a relatively high normalized emittance of 5×10^{-2} mm mrad $\sqrt{\text{MeV}}$.

The electrode geometry used in our experiment to extract the ions consists of a pair of parallel-plate electrodes held at different potentials. One of the electrodes has an aperture through which the ion beam can pass. The MOT is situated between the two electrodes, so that as the ions are created, they are accelerated toward the aperture by the uniform electric field created by the voltages applied to the electrodes. As the ions approach and pass through the aperture, they experience a slight electric field curvature that has a weak diverging effect. This defocusing is a manifestation of a special form of *Davisson-Calbick* lens [25] formed by our electrode geometry that has useful properties for determining the emittance of the source, as will be discussed below.

A unique experimental configuration is necessary to ensure that the electrode geometry for the extraction lens is compatible with the laser geometry required to create a MOT. This is accomplished with specially constructed electrodes made from two fused silica optical flats that are 100 mm in diameter and 9.5 mm thick. The optical flat serving as the extraction electrode has a 3 mm diameter hole drilled through the center and is coated with a roughly 150 nm thick layer of aluminum on the side facing the MOT. This electrode acts as a mirror with $\approx$ 94% reflectance at 425 nm (the wavelength of the MOT lasers) and is held at ground potential via the connection to the vacuum chamber. The side of the second window facing the MOT is coated with a thin layer of indium tin oxide, which is a

transparent conductor that acts as the second electrode. The other side is coated with an antireflective coating, giving a total transmittance for the window of 97% at 425 nm. This electrode is electrically isolated from the vacuum chamber and is connected to a high voltage power supply which defines the extraction voltage. With the two electrodes held 1.5 cm apart, the six beam MOT geometry can be accommodated by reflecting two of the beams off the mirrored electrode, as shown in Figure 1. In this configuration, the MOT is located half way between the two electrodes, and hence an ion beam with energy equal to one half the extraction voltage is created.

After exiting the aperture in the grounded electrode, the ion beam propagates in a field-free drift region for a distance of approximately 1.2 m before reaching a detector for measuring the spatial profile of the beam. The detector is an image-intensifying phosphor screen that consists of a multichannel plate followed by a phosphor screen. The image of the beam on the phosphor screen is captured with a cooled CCD camera. A typical beam image is shown in Figure 2. Note the image reflects the long, narrow geometry of the ionization region resulting from the focused UV ionization laser beam passing through the MOT. We determine the emittance in the horizontal direction, $\varepsilon_{rms,x}$, where the width is defined primarily by the width of the ionization laser beam. Also shown in Figure 2 is an ion beam profile corresponding to the integrated image of the beam along the vertical direction. We fit a Gaussian curve to this profile to extract the beam width.

If the ion source is operated in a continuous mode, the resulting ion beam must propagate through the quadruple magnetic field used to create the MOT. This field acts as a weak astigmatic lens element focusing the ion beam in one direction while defocusing it in the orthogonal direction [13]. While this effect is small and could be corrected by additional ion-optic elements, its influence was eliminated in our measurements by operating in a pulsed mode as follows. The MOT was turned on and allowed to collect and cool atoms for long enough to approach continuous-mode densities, typically 400 ms, at which point the magnetic fields and laser beams were switched off. After 240 μs the current in the magnetic field coils had decayed to below 1% of its steady-state value, and the MOT and photoionization beams were switched back on for 10 ms, which was sufficient time to ionize nearly all

of the atoms in the MOT. In this way the ions were created and extracted after the quadrupole field had been extinguished. The system remained off for approximately 90 ms before repeating the cycle. Images were typically integrated over many pulses to accumulate sufficient signal-to-noise, with total camera exposure times between 100 s and 600 s, corresponding to an integration of between 200 pulses and 1200 pulses.

The emittance of the beam was investigated by conducting a series of measurements of its spatial profile at the detector as a function of the extraction voltage. These measurements give direct information on the emittance because the *Davisson-Calbick* lens as it is implemented here has the special property that the focal length is independent of the extraction voltage. The key to this independence is the fact that the ions are created in the region between the plates of the lens. As the voltage is increased, the gradient at the aperture becomes larger, but this effect is cancelled by the higher kinetic energy of the ions as they pass through the aperture.

Because of this voltage-independent focal length, one might expect a beam emerging from the extraction electrode to experience no change in spatial profile at the detector as the extraction voltage is varied. This is in fact true for a beam with zero emittance. If the ion beam has a finite emittance, however, the beam size does depend on extraction voltage. As the voltage is lowered, the conservation of normalized emittance requires the angular spread of the source to increase, since the source size remains constant. This increased angular spread shows up as an increase in beam size at the detector. By combining measurements of the voltage dependence of this beam size change with appropriate modeling of ion trajectories we are able to make estimates of the emittance of the beam.

Beam size versus voltage measurements were carried out under several sets of conditions. In each case, the beam widths were normalized by dividing by the average of the beam widths measured at extraction voltages above 2 kV, where the beam energy is high enough that the width is essentially constant. This normalization was done to allow for comparison between the different experimental configurations, where slight variations in ionization beam size, and hence source size, occurred.

Uncertainties in the beam width measurements were predominantly due to random variations, caused for the most part by small fluctuations in ionization laser position. To estimate the size of these uncertainties we took 10 measurements at a fixed extraction voltage and calculated the standard deviation. This standard deviation is represented by error bars in Figure 3, where the assumption is made that the fluctuations were the same for all extraction voltages. We note that the magnitude of this uncertainty corresponds to ± 2% of the measured value.

Figure 3a shows beam width measurements as a function of extraction voltage under close to optimum conditions. In this case, the MOT parameters were adjusted to obtain the lowest temperature possible, which we measured to be $(120 \pm 50)\ \mu\text{K}$, and the wavelength of the ionizing laser was fixed at a detuning of $\Delta\lambda = (0.10 \pm 0.02)\ \text{nm}$ above threshold. At this detuning, this increases the effective ion cloud temperature to $(190 \pm 60)\ \mu\text{K}$. As seen in the figure, under these conditions the beam undergoes no measurable change in size over the entire range of extraction voltages down to 50 V (corresponding to a beam energy of 25 eV). This measurement is consistent with zero emittance, and so only allows us to put an upper bound on the emittance of the beam.

Since no observable increase in beam size at low voltage is seen in the data in Figure 3a, it is important to test the level of sensitivity of our measurements to non-zero emittance values. In order to do this we artificially increased the emittance of the source by increasing the temperature of the ions in two separate ways.

For the beam width measurements in Figure 3b, the ion temperature was increased by increasing the MOT temperature, while the ionization laser was kept at the same small detuning as in Figure 3a. A higher MOT temperature of $(1.20 \pm 0.10)\ \text{mK}$ was achieved by loading and extracting while a switching transient was still present in the magnetic field, and the associated increase in emittance is reflected in the data. As the extraction voltage is reduced below 100 V, the beam width shows a measurable increase, and by 50 V, the beam width has increased by 10% over the high extraction voltage values. This is a clear sign that the emittance is greater at higher MOT temperatures, and is an indication of the sensitivity of our measurement.

In Figure 3c, the MOT temperature was maintained at the optimal $(120 \pm 50)\ \mu\mathrm{K}$, but the ions were made hotter by tuning the ionization laser significantly above threshold. For this data, the wavelength of the ionization laser was set (1.04±0.02) nm above threshold, providing an additional (1.48±0.03) mK of energy to the ions. As in Figure 3b, when the extraction voltage goes below 100 V the beam size starts to increase, going up by over 10% at a voltage of 50 V. This increase at low beam energy shows that the emittance is greater than in Figure 3a, as expected for the higher ion temperature.

In order to quantitatively evaluate the significance of the measurements shown in Figure 3 in terms of the emittance of the beam, it is necessary to model the system using a ray tracing simulation. Starting with a source size that is known through measurements of the ionization laser profile, an initial temperature that is measured by MOT expansion, and knowledge of the physical dimensions of the extraction geometry, it is possible to uniquely predict all the ion beam characteristics, including its emittance and its size at the detector. By comparing the predicted beam size with the measured values we gain confidence that the emittance derived from the calculation is an accurate reflection of the true beam emittance.

The simulations were done with a finite difference electric field calculation based on a realistic model of the electrode geometry and a fourth-order Runge-Kutta equation-of-motion calculation to determine the trajectories for 10 000 ions. The ions were given a spherically symmetric Gaussian spatial distribution with a $1/e^2$ radius of ≈ 10 μm, corresponding to the measured beam waist of the ionization laser. A Maxwell-Boltzmann energy distribution corresponding to the measured temperature of the MOT was ascribed to the ions. Space charge effects were not included in the simulations.

The results of the simulation are shown in Figure 3 along with the measured data. For Figure 3a, the ions were given an initial energy distribution corresponding to a temperature of 190 μK. This value was arrived at by combining the MOT temperature of 120 μK with the additional ionization energy of 150 μK in quadrature. The width of the simulated beam was determined at a position corresponding to the detector in the experiment for a series of extraction voltages between 30 V and 12 kV and normalized in the same manner as the experimental data. We see excellent agreement between the simulation and the

11

measurements, with the simulation showing only a slight rise in beam size at the lowest extraction voltage by an amount smaller than the uncertainties of the measurement. The *rms* emittance of the simulated beam was determined from its spatial and angular distributions via Equation 2 at a position 1 mm downstream from the source location using an extraction voltage of 5 kV. The value obtained from this calculation was 6.0×10^{-7} mm mrad $\sqrt{\text{MeV}}$.

In order to estimate how accurately this simulation-based emittance reflects the actual emittance of our source, similar calculations were performed on simulations using the elevated temperature conditions present during the width measurements in Figures 3b and 3c. For Figure 3b, the simulation was done with an initial temperature of 1.21 mK, which is the quadrature sum of the measured temperature of the atom cloud and the additional ionization energy of 150 μK. Again, there is excellent agreement between the simulation and the data. The simulated beam in this case had a numerically calculated emittance of 1.55×10^{-6} mm mrad $\sqrt{\text{MeV}}$. Likewise, in Figure 3c, excellent agreement is seen between the data and the simulation, which was performed with an initial temperature of 1.48 mK, corresponding to the quadrature sum of the thermal energy and the additional energy added to the system by being 1 nm above ionization threshold. For this case the simulated beam had a numerically calculated emittance of 1.60×10^{-6} mm mrad $\sqrt{\text{MeV}}$.

Taken all together, the excellent agreement between simulation and experiment in all cases of Figure 3 suggests that with the measured MOT temperature, the known electrode geometry and the measured UV beam profile as inputs, the simulation accurately describes the observed behavior of the ion beam created by the MOTIS described here. Further simulations show that if the temperature was assumed to be 350 μK rather than 190 μK in the optimal case of Figure 3a, then the deviation of the simulated normalized beam width from unity would begin to exceed the uncertainties of the measurements at the lowest extraction voltages. For this case of marginal agreement the calculated emittance of the simulated beam was 8.2×10^{-7} mm mrad $\sqrt{\text{MeV}}$. So the best estimate of the emittance for the MOTIS described here is 6.0×10^{-7} mm mrad $\sqrt{\text{MeV}}$ with an upper bound of 8.2×10^{-7} mm mrad $\sqrt{\text{MeV}}$. We

would not expect an emittance much smaller than the simulated value, though such a value would be consistent with the beam width measurements.

Once the emittance of the source is measured, the brightness can be derived from a simple measurement of the current in the beam. This was done by placing a Faraday cup in the beam path, approximately 50 cm from the source. The power in the ionization laser was set at approximately 4 mW, well above the observed ionization saturation level. A detuning of $\Delta\lambda = (1.04 \pm 0.02)$ nm was used and the source was operated in continuous mode with an extraction voltage of 10 keV. Subsequent measurements showed that the current is independent of detuning when the ionization process is fully saturated and also that the current does not depend on extraction voltage.

As mentioned previously, the total current in the ion beam was expected to depend on the density of atoms in the MOT. To demonstrate this the peak density at the center of the MOT was evaluated under several different loading conditions by measuring both the size of the MOT via a CCD camera image of the fluorescence and the atom number in the MOT via fluorescence intensity measurements. The density values for the measurement had an uncertainty of 20% due to the uncertainty of the atom number in the MOT brought about by uncertainties in the laser power in the MOT beams inside the vacuum chamber and the collection efficiency of the imaging optics. Figure 4 shows the linear dependence of the extracted ion current on MOT density as predicted in Reference [19], with a proportionality constant of $(9.4 \pm 0.4) \times 10^{-10}$ pA atoms^{-1} cm^{3}.

The largest current we have been able to extract from the present source is (1.40 ± 0.03) pA. This limit is due in part to the peculiarities of chromium, which is known to be limited in MOT density to approximately 10^{9} atoms cm^{-3} because of light-assisted collisions [20]. For other elements, the maximum densities achieved via laser cooling are of the order 10^{11} atoms cm^{-3} and are ultimately limited by collisions and radiation pressure [21]. Using the proportionality constant determined from Figure 4 to extrapolate the measured current for the present source to these higher densities suggests that it should be possible to extract as much as 100 pA out of a MOTIS, depending on the element.

We should note that the measured current of Figure 4 is for the whole beam. As can be seen in Figure 2, the beam has an elongated shape for reasons discussed above. For most uses, a symmetric beam is preferred and could be achieved by placing an aperture in the beam path at the expense of a decreased current. To estimate the effect of an aperture, we take a typical beam profile, as shown in Figure 2, and mask the beam such that the width is the same in both directions. This leads to an effective square-beam current of approximately 0.25 pA for the maximum density achieved with the present source. Using this apertured square-beam current and the *rms* emittance of 6.0×10^{-7} mm mrad $\sqrt{\text{MeV}}$, Equation 3 gives a brightness of 0.88 A cm^{-2} sr^{-1} eV^{-1}.

While the above considerations result in a conservative estimate of the MOTIS brightness for the present realization, the actual brightness of a beam generated in such a source can be increased by further aperturing the beam. This is because the phase space distribution of ions is Gaussian, and as long as the aperture selects a region that is not very small compared to the width of the distribution, the reduction in emittance is more significant than the reduction in current. Based on this, a core brightness as high as 2.25 A cm^{-2} sr^{-1} eV^{-1} can be obtained in the present system before further reduction in aperture size stops yielding a higher value. If we extrapolate this calculation to what might be possible in a system where higher currents are possible due to higher densities, a core brightness of ≈ 200 A cm^{-2} sr^{-1} eV^{-1} should be possible. This brightness compares quite favorably with that of a LMIS, which is typically reported to be 10 A cm^{-2} sr^{-1} eV^{-1} to 100 A cm^{-2} sr^{-1} eV^{-1}.

By knowing the emittance and brightness of an ion source, it is possible to predict how well the extracted beam can be focused and how much current will be delivered to the spot. Given the values determined here, we can predict that it should be possible to create an ion beam with a focus of less than one nanometer and a beam current of several picoamperes, assuming a collimated beam with a width of 20 μm is focused using a lens with a working distance of ≈ 5 mm and a spherical aberration coefficient of 250 mm. A beam of this sort would be ideal for use in light-ion microscopy where the working distance is similar to what has been used in high resolution scanning electron microscopes.

In conclusion, we have demonstrated that the MOTIS is a low emittance, high brightness ion source suitable for focused ion beam applications. We have created a high quality beam with an estimated *rms* emittance as low as 6.0×10^{-7} mm mrad $\sqrt{\text{MeV}}$, and we have extracted approximately 0.25 pA of usable current, giving rise to a normalized brightness of 0.88 A cm^{-2} sr^{-1} eV^{-1}. With future improvements it may be possible to increase the brightness as high as 200 A cm^{-2} sr^{-1} eV^{-1}, allowing subnanometer resolution with several tens of picoamperes of current.
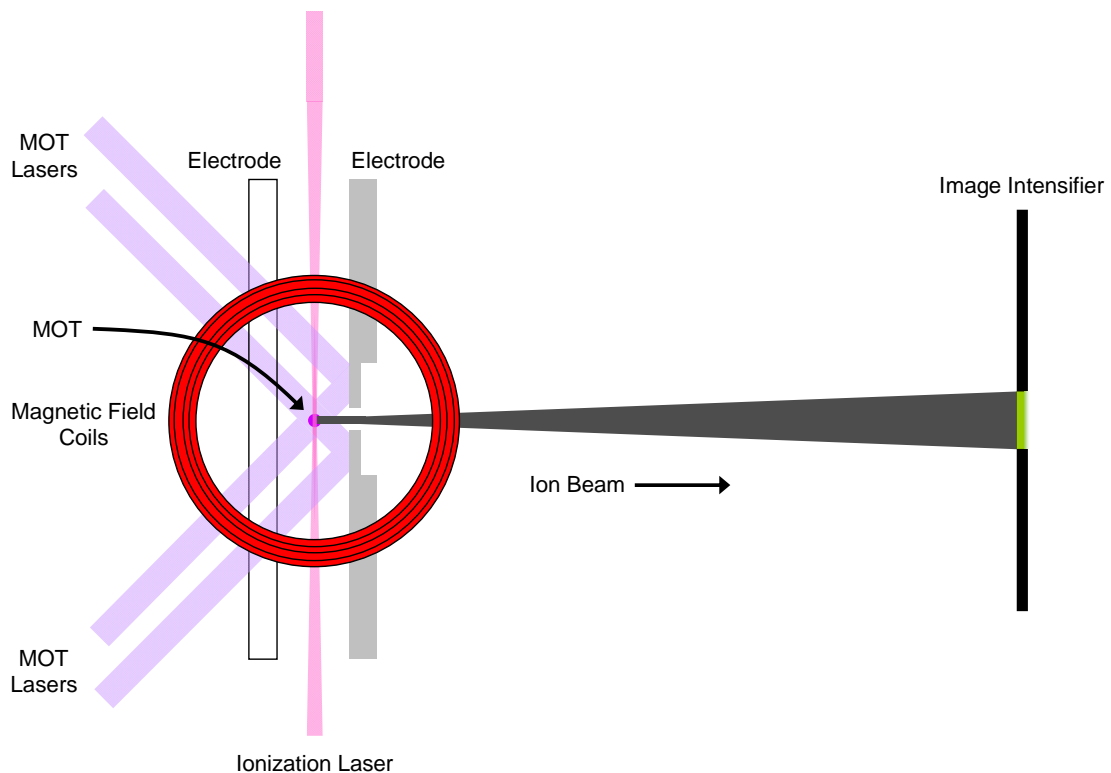
FIGURE 1. Schematic of the apparatus. A magneto-optical trap (MOT) is formed between two electrodes, one of which has a mirrored surface, the other consisting of a fused silica optical flat with a

transparent conductive coating. Four of the six laser beams necessary to form the MOT pass through the window and reflect from the mirrored electrode as shown. Another pair of MOT beams (not shown) is perpendicular to the page. The magnetic field of the MOT is generated by a pair of coils. An ionization laser intersects the MOT, and ions are created and extracted through a hole in the mirrored electrode. The ion beam propagates in a field-free drift region and is detected with a multichannel plate-intensified phosphor screen.
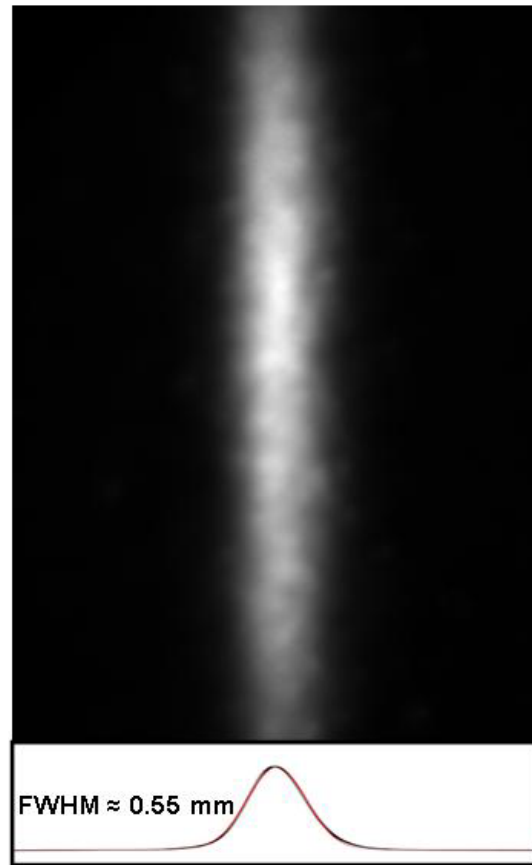

FIGURE 2. CCD image of the ion beam on the phosphor screen. Also shown (black curve) is a profile obtained by integration of the image in the vertical direction. The red curve is a Gaussian fit to the integrated curve, giving a full width half maximum (FWHM) value of approximately 0.55 mm.
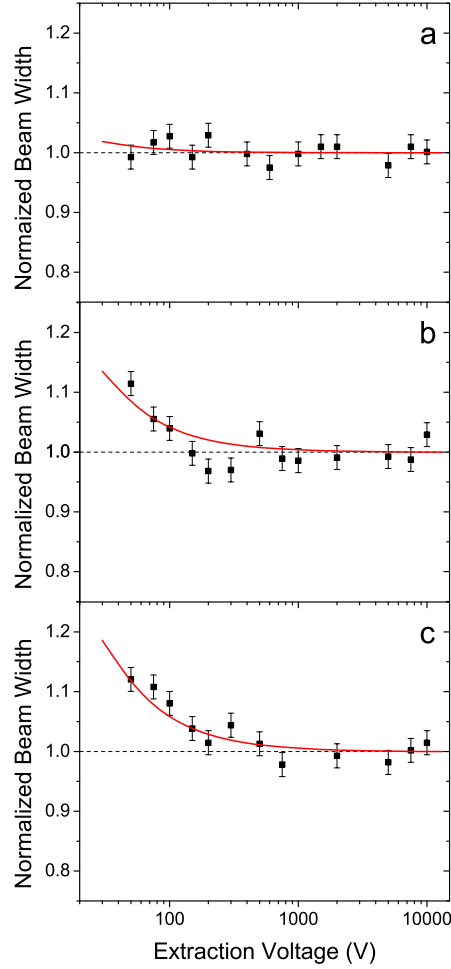
FIGURE 3. Ion beam width measurements as a function of beam extraction voltage. In all three panels, the beam widths were normalized to the average of the high extraction voltage values, and a dashed line at a normalized beam width of 1 has been added for clarity. Error bars represent one standard deviation of 10 width measurements. a) Optimum configuration with T = (120±50) μK for the MOT, $\Delta\lambda = (0.10 \pm 0.02)$ nm, T = (190±60) μK for the ions. The red curve is a numerical simulation corresponding to a beam of the same initial size and an emittance of 6.0×10^{-7} mm mrad $\sqrt{\text{MeV}}$. b) Temperature artificially increased in MOT, with T = (1.20±0.10) mK for the MOT, $\Delta\lambda = (0.10 \pm 0.02)$ nm, T = (1.21±0.10) mK for the ions. The red curve is a numerical simulation

corresponding to a beam of the same initial size and an emittance of 1.55×10^{-6} mm mrad $\sqrt{\text{MeV}}$. c) Ion temperature artificially increased, with T = (120±50) µK for the MOT, $\Delta\lambda = (1.04 \pm 0.02)$ nm, T = (1.48±0.06) mK for the ions. The red curve is a numerical simulation corresponding to a beam of the same initial size and an emittance of 1.60×10^{-6} mm mrad $\sqrt{\text{MeV}}$.
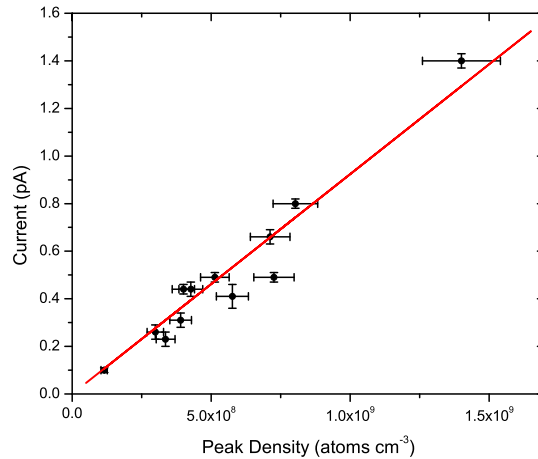

FIGURE 4. Extracted current as a function of peak MOT density. The red line is a linear fit to the data with a proportionality constant of $(9.4 \pm 0.4) \times 10^{-10}$ pA atoms^{-1} cm^3. We have extracted a maximum current of (1.40 ± 0.03) pA.

REFERENCES

[1] Melngailis, J. *J. Vac. Sci. Technol. B* **1987**, *5*, 469.

[2] Orloff, J. *Rev. Sci. Instrum.* **1993**, *64*, 1105.

[3] Giannuzzi, L. A.; Stevie, F. A. *Introduction to Focused Ion Beams: Instrumentation, Theory, Techniques, and Practice*; Springer: New York, 2005.

[4]   Orloff, J.; Utlaut, M.; Swanson, L. *High Resolution Focused Ion Beams: FIB and Its Applications*; Kluwer Academic/Plenum Publishers: New York, 2003.

[5] Tondare, V. N. *J. Vac. Sci. Technol. A* **2005**, *23*, 1498.

[6] Kalbitzer, S.; Knoblauch, A *Rev. Sci. Instrum.* **1998**, *69*, 1026.

[7] Ward, B. W.; Notte, J. A.; Economou, N. P. *J. Vac. Sci. Technol. B* **2006**, *24*, 2871.

[8] Leclerc, S.; Declemy, A.; Beaufort, M. F.; Tromas, C.; Barbot, J. *J. Appl. Phys.* **2005**, *98*, 113506.

[9] Hanssen, J. L.; McClelland, J. J.; Dakin, E. A.; Jacka, M. *Phys. Rev. A* **2006**, *74*, 063416.

[10] Claessens, B. J.; van der Geer, S. B.; Taban, G.; Vredenbregt, E. J. D.; Luiten, O. J. *Phys. Rev. Lett.* **2005**, *95*, 164801.

[11] Freinkman, B. G.; Eletskii, A. V.; Zaitsev, S. I. *Microelectron. Eng.* **2004**, *73-74*, 139.

[12] Hill, S. B.; McClelland, J. J. *App. Phys. Lett.* **2003**, *82*, 3028.

[13] Reiser, M. *Theory and Design of Charged Particle Beams*; Wiley-VCH: Weinheim, 2004.

[14] Ward, J. W. *J. Vac. Sci. Technol. B* **1985**, *3*, 207.

[15] Seliger, R. L.; Ward, J. W.; Wang, V.; Kubena, R. L. *Appl. Phys. Lett.* **1979**, *34*, 310.

[16] Alton, G. D.; Read, P. M. *J. Appl. Phys.* **1989**, *66*, 1018.

[17] Loffelmacher, D.; Adamczewski, J; Stephan, A.; Meijer, J.; Rocken, H.; Bukow, H. H.; Rolfs, C. *Nucl. Instr. Meth. in Phys. Res. B* **1998**, *139*, 422.

[18] Raab, E. L.; Prentiss, M.; Cable, A.; Chu, S.; Pritchard, D. E. *Phys. Rev. Lett.* **1987**, *59*, 2631.

[19] van der Geer, S. B.; Reijnders, M. P.; de Loos, M. J.; Vredenbregt, E. J. D.; Mutsaers, P. H. A.; Luiten, O. J. *J. Appl. Phys.* **2007,** *102*, 094312.

[20] Bradley, C. C.; McClelland, J. J.; Anderson, W. R.; Celotta, R. J. *Phys. Rev. A* **2000**, *61*, 053407.

[21] Metcalf, H. J.; van der Straten, P. *Laser Cooling and Trapping*; Springer-Verlag: New York, 1999.

[22] Mainfray, G.; Maus, C. *Multiphoton Ionization of Atoms*; Academic Press: Orlando, FL, 1984.

[23] Killian, T. C. *Science* **2007**, *316*, 705.

[24] Claessens, B. J.; Reijnders, M. P.; Taban, G.; Luiten, O. J.; Vredenbregt, E. J. D. *Phys. Plasmas* **2007**, *14*, 093101.

[25] Klemperer, O. *Electron Optics*; Cambridge University Press: New York, 1953.